Research Article | Vol. 31, No. 24 / 20 Nov 2023 / Optics Express 40525
Optics EXPRESS

Numerical analysis of micro-optics based single photon sources via a combined physical optics and rigorous simulations approach

CARLOS JIMENEZ,[1,*] CHRISTIAN HELLMANN,[2] ANDREA TOULOUSE,[1] JOHANNES DROZELLA,[1] FRANK WYROWSKI,[3] AND ALOIS HERKOMMER[1]

[1] *Institute for Applied Optics (ITO), University of Stuttgart, 70569 Stuttgart, Germany*
[2] *Wyrowski Photonics GmbH, Jena, Germany*
[3] *Applied Computational Optics Group, Friedrich Schiller University Jena, Jena, Germany*
[*] *jimenez@ito.uni-stuttgart.de*

Abstract: The use of 3D printed micro-optical components has enabled the miniaturization of various optical systems, including those based on single photon sources. However, in order to enhance their usability and performance, it is crucial to gain insights into the physical effects influencing these systems via computational approaches. As there is no universal numerical method which can be efficiently applied in all cases, combining different techniques becomes essential to reduce modeling and simulation effort. In this work, we investigate the integration of diverse numerical techniques to simulate and analyze optical systems consisting of single photon sources and 3D printed micro-optical components. By leveraging these tools, we primarily focus in evaluating the impact of different far-field spatial distributions and the underlying physical phenomena on the overall performance of a compound micro-optical system via the direct evaluation of a fiber in-coupling efficiency integral expression.

1. Introduction

Reliable and high-quality single photon sources are crucial for scaling quantum information technology systems used in computing and encrypted communication channels [1]. In order to take full advantage of what single photon sources(SPS) can provide, it is important to maximize the portion of photons being extracted and coupled into optical waveguides or single mode fibers(SMF). There exist different proposals for coupling photons from SPSs into SMFs [2,3]. Nevertheless, some of these methods rely on large objectives in addition to complex positioning systems, which effectively limit the number of addressable emitters without increasing the overall space complexity. Such limitations can be circumvented with the help of 3D printed micro optical components [4]. In addition to facilitating compact integrated systems and direct coupling into optical fibers, these elements benefit from a process with an inherent high degree of spatial resolution that enables the use of a large variety of surface profiles [5,6].

Most of these 3D printed components are designed via ray-tracing based software packages. Differently, systems such as the ones involving SPSs cannot be accurately described with tools based on geometrical optics. For these, rigorous simulation methods are needed in order to extract all field components and evaluate the fields' interactions with the nano-photonic structures [7]. Nevertheless, relying on these methods for obtaining far-field information from nano structure systems or for propagating field components through additional optical elements can result in large computational overheads, severely impacting the efficiency of such approach.

#502926 https://doi.org/10.1364/OE.502926
Journal © 2023 Received 9 Aug 2023; revised 23 Oct 2023; accepted 7 Nov 2023; published 15 Nov 2023

Optics EXPRESS

As an alternative, in this work we explore the combination of rigorous simulation methods and physical optics solvers being efficiently applied to specific sub-sections of an optical system consisting of SPSs and multiple micro-optical interfaces. Finally, we compare the obtained results to the ones derived from standard point source models in combination with ray-tracing analysis. Accordingly, the present letter is then structured as follows: On Sec. 2 the use of 3D printed optics as interfacing elements to SPSs is reviewed. Sec. 3 presents all relevant details behind the numerical modeling and implementations used in the present publication. Consequently, the obtained results are then presented and analyzed on Sec. 4 and to finalize conclusions are given on Sec. 5.

2. 3D printed optics for single photon sources

Different SPS architectures have been demonstrated for which high collection efficiencies were obtained by using standard optical objectives [8,9]. Differently from such objectives, SMFs are characterized by their limited NA values, making the direct interfacing between SPSs and SMFs more challenging. In this regard, various methods have been proposed which include the use of compound lens systems [2], direct high NA fiber coupling [3] and photonic crystals based SMF schemes [10].

In addition to these, the use of 3D printed micro optical elements has been proposed as an alternative coupling strategy [4,7,11]. This approach benefits from the versatility offered by available 3D printing technologies, specifically the ones based on multiphoton polymerization that allow the fabrication of different micro-optical interfaces such as free form surfaces [6], aspheres and diffractive lenses [12]. In this manner, it is possible to obtain a significant reduction in overall system size, reduced optical losses with the help of anti reflection coatings [13] and increased fiber coupling efficiencies facilitated by optical interfaces tailored to the emitter's field characteristics. 3D printed optics can therefore provide access to the possibility of interfacing multiple single photon emitters without representing a significant increase in spatial requirements, which is of great importance for scaling up different quantum technology systems [14].

Differently from SPS nano-photonic systems, 3D printed micro optical components are usually designed via non-rigorous approaches. One conventional and commonly used method is ray-tracing, which facilitates the design of complex micro optical systems consisting of multiple interfaces [15,16]. Ray-tracing exploits the principles behind geometrical optics and benefits from a reduced computational demand in contrast to rigorous numerical methods. Nevertheless, ray-tracing fails in providing accurate results for situations in where diffraction plays a significant role and in the evaluation of field components within focal regions.

Here is where physical optics based numerical implementations provide a solution to overcome these limitations. Methods such as the angular spectrum method (ASM), the Rayleight-Sommerfeld convolution method (RSC) and others can be utilized for propagating field components through homogeneous regions of space [17] whereas the propagation across optical interfaces can be performed via the thin-element approximation (TEA) or other higher order methods [18,19].

3. Modeling techniques

3.1. Dipole emitter - FDTD simulations

A common way of describing single photon emitters is via the dipolar approximation [20]. In this way, a single photon emitter is represented as an oscillating current density for which all generated field components can be obtained by means of numerical methods that support the definition of point-like current sources such as the finite element method (FEM), Fourier domain based methods [21,22] or the finite-differences-time-domain (FDTD) technique. All near-field components evaluated in the present publication were extracted through a cylindrical coordinates

Optics EXPRESS

FDTD implementation via the open source software package Meep [23]. In this coordinate system, the total electric field can be expressed using a Fourier modes series expansion

$$\mathbf{E}_c(\mathbf{r}) = \sum_{m=-\infty}^{\infty} \mathbf{E}_m(r,z)e^{im\phi} \tag{1}$$

for which in case of a dipole emitter positioned at the symmetry axis, i.e, $\vec{r}_{QD} = (0,0,z)^T$, only the m=-1,0,1 Fourier modes contribute to the electric field expansion [20]. These cylindrical components can then be used for expressing the near-field in terms of Cartesian coordinates via the following linear transformations

$$\begin{aligned} E_x(\mathbf{r}) &= \cos\phi E_\rho(\mathbf{r}) - \sin\phi E_\phi(\mathbf{r}) \\ E_y(\mathbf{r}) &= \sin\phi E_\rho(\mathbf{r}) + \cos\phi E_\phi(\mathbf{r}) \end{aligned} \tag{2}$$

Rigorous simulation methods such as FDTD can demand a large amount of computational resources and their use is usually restricted to the extraction of relevant near-field information. For situations in where homogeneous open space far-field characteristics are needed, appropriate efficient computational approaches are preferable. In this case, far-field components can be obtained by means of a near-to-far-field transformation [24], by exploiting the field's angular representation in combination with the method of stationary phase [25] or via the generalized far-field integral [26].

3.2. Micro-optical system - physical optics simulations

Following, the obtained near-field components need to be propagated through optical systems like the one shown in Fig. 1(a). This system was optimized via standard sequential ray-tracing methods using a point source with a Gaussian-like amplitude distribution in accordance to the design approaches utilized in [4,11] and [27]. The light collected from the point-like element is redirected to a single mode fiber, represented on the diagram as a vertical plane. In this case, a hemispherical solid immersion lens (h-SIL) in direct contact with a GaAs semiconductor layer is considered. SILs have attracted significant attention due to their ability to enhance spatial resolution, improve extraction from point-like emitters and provide higher magnification, thereby facilitating better interaction with nano-scale structures or emitters [11,28]. The middle component corresponds to a plano-convex aspherical lens, optimized with the goal of generating a collimated set of rays. Lastly, as for the fiber-lens, it consists of an aspheric surface profile designed for producing a diffraction-limited focal spot. Its focusing half-angle of incidence was determined from a SMF's numerical aperture with a value of 0.12. All relevant design parameters corresponding to the used micro-optical components shown in Fig. 1(a) can be found in Supplement 1.

Figure 1(b) shows a diagram representing all operations involved in the propagation of each field component through the system. To start, the obtained FDTD near-field distributions are propagated from the source plane towards the h-SIL via generalized far-field integral evaluations. For situations in where strong wavefront phase profiles are encountered, as in the case of the dipole sources discussed here, relying on the generalized far-field integral benefits from the use of pointwise inverse Fourier transforms (IPFT) [29] which results in a significantly reduced computational demand in comparison to other approaches such as the ASM or the RSC method [26].

Following, the plano-convex lens field response can be obtained as

$$\mathbf{E}^D(\boldsymbol{\rho}^D; z^D) = \hat{\mathbf{M}}(\boldsymbol{\rho}^D, \boldsymbol{\rho}^C; \Delta z)\, \mathbf{E}^C(\boldsymbol{\rho}^C; z^C) \tag{3}$$

in where $\boldsymbol{\rho} = (x, y)$ is defined over each evaluation plane located at z, $\mathbf{E}^C(\boldsymbol{\rho}^C; z^C)$ stands for the obtained input far-field components generated by the h-SIL, $\mathbf{E}^D(\boldsymbol{\rho}^D; z^D)$ represents the lens output

Optics EXPRESS

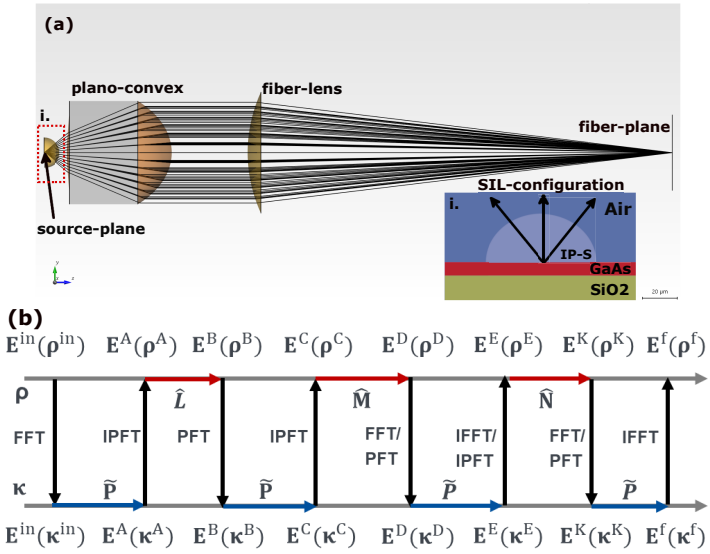

Fig. 1. (a) Schematic representation of the optical system utilized for propagating the obtained near-field components shown in Fig. 2. (b) Field-tracing diagram. At every plane, each field component is connected to its Fourier domain representation (with $\boldsymbol{\kappa}$ representing coordinates in Fourier domain) via different types of Fourier transforms.

field response and $\hat{\mathbf{M}}(\boldsymbol{\rho}^D, \boldsymbol{\rho}^C; \Delta z)$ corresponds to the operator connecting these two. This last consists of the local plane interface approximation (LPIA) [19,30,31] operator in combination with a frequency domain free space propagation kernel $\tilde{\mathbf{P}}$ previously introduced as the ASM. As for the fiber-lens, its output field is obtained via the $\hat{\mathbf{N}}(\boldsymbol{\rho}^K, \boldsymbol{\rho}^E)$ operator which embeds only the LPIA functionality. Finally, the fiber-lens output field is free-space propagated towards its focal plane in where the real space field components are given by $\mathbf{E}^f(\boldsymbol{\rho}^f; z^f)$. It must be mentioned that differently from the far-fields obtained by means of IPFTs, the fiber-lens focal field components are obtained via standard IFFTs, since at focal regions, the use of pointwise transformations is not valid anymore [29]. Such a combination of standard and pointwise transform operations allows an efficient and robust full-vectorial field extraction strategy, exploiting where possible the inherent field characteristics.

At the fiber plane, the obtained $\mathbf{E}^f(\boldsymbol{\rho}^f; z^f)$ field components are compared against a fiber-field mode which is approximated by a Gaussian-like distribution. This comparison is carried out by evaluating the following overlap integral expression

$$\eta = \frac{\iint_{\mathbb{R}^2} E_{x,f} E^*_{x,ref}\, dx\, dy}{\iint_{\mathbb{R}^2} |E_{x,f}|^2\, dx\, dy \iint_{\mathbb{R}^2} |E_{x,ref}|^2\, dx\, dy} \tag{4}$$

in where $E_{x,f}$ represents the fiber-lens focal plane E_x component, $E_{x,ref}$ the reference SMF field and $E^*_{x,ref}$ its complex conjugate. In this publication, the far-field evaluations and the subsequent propagation and evaluation steps were conducted using VirtualLab Fusion (VLF) [32] which is a software package that offers an unified framework for analyzing optical systems and facilitates the division of such into manageable sub-sections, over which dedicated Maxwell solvers can be applied. VLF and its usage has been demonstrated through a large collection of publications and differently from software packages based on purely ray-tracing or rigorous methods, it enables an efficient approach of simulating and modeling optical systems in where the involved physical dimensions vary over various orders of magnitude [19,30,31]. The inherent modularity of our

Optics EXPRESS

proposed combined approach makes it possible to replace any component shown in Fig. 1(a) with other suitable micro-optical interface or source model, enabling more flexibility in the type of system that can be modeled.

4. Results

4.1. Dipole source within flat semiconductor layer

4.1.1. FDTD based near-field evaluation

Figure 2(a) presents a schematic representation of the first system being modeled. This consists of a dipole emitter embedded within a flat GaAs (n=3.5325) layer with a thickness of 260 nm, below which a 200 nm thin SiO2 (n=1.4518) layer is positioned with a perfect electric conductor (PEC) boundary condition applied to it. Above the GaAs layer, a homogeneous region of space with a refractive index value equal to 1.53 (IP-S photoresist,Nanoscribe GmbH, Karlsruhe, Germany) at a wavelength of 900 nm is included. Finally, perfectly match layer (PML) sections are applied to the top and right boundaries. For such an emitter-material configuration, it is widely known that the generated near-field components highly depend on the emitter's relative position with respect to the interfaces [25]. This can also be observed in Fig. 2 which presents E_x near field distributions for a dipole offset value of 50 and 130 nm.

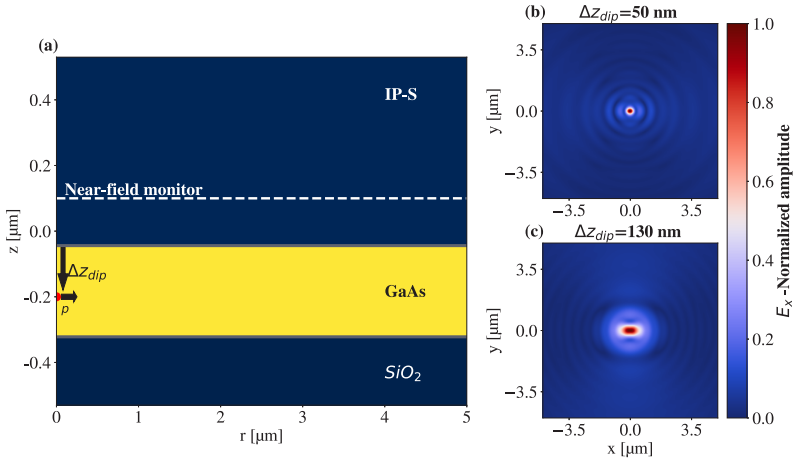

Fig. 2. (a) Schematic representation of a flat material distribution in cylindrical coordinates. Δz_{dip} stands for the dipole's z offset with respect to the upper GaAs interface. (b) and (c) Normalized E_x components extracted via a FDTD near-field monitor, at a distance of 150 nm from the GaAs upper interface for two different Δz_{dip} values.

4.1.2. Micro-optical system - propagation of field components

In this section, we provide the results of propagating the obtained near-field components from Sec. 4.1.1 through the micro-optical system presented in Fig. 1(a). To start, in Fig. 3 we present a far-field E_x comparison between components obtained directly through the FDTD solver and via the generalized far-field integral approach. Similarly to the far-field amplitude distributions shown in Fig. 3(a) and (b), Fig. 3(d) and (e) present the associated unwrapped phase profiles. In Fig. 3(f) we compare these phase distributions to the phase term of an ideal spherical wave, demonstrating the validity of relying on the generalized far-field integral for extracting far-field components from the obtained FDTD near-field information in agreement to what is presented in [26].

Optics EXPRESS

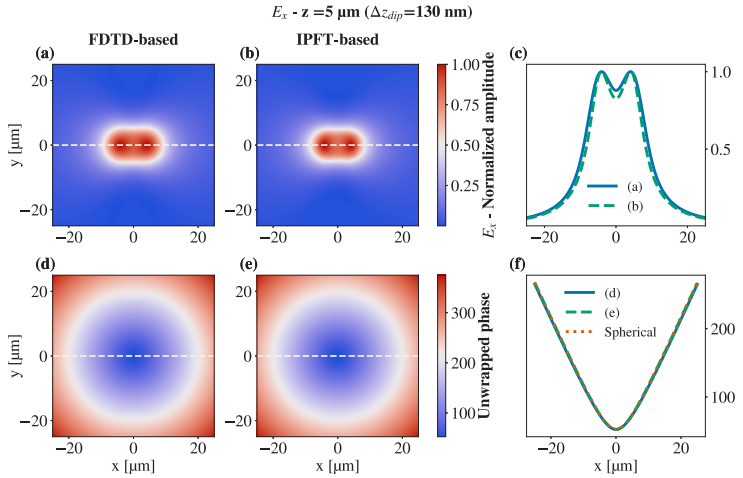

Fig. 3. (a),(b) present E_x far-field distributions obtained directly from the FDTD solver and via the generalized far-field integral approach. (d),(e) show the associated unwrapped phase profiles and (c) and (f) presents cross-section comparisons for the amplitude and unwrapped phase distributions.

Figure 4 presents E_x field distributions product of the used FDTD near-field source components evaluated at the entrance of the fiber-lens ($\mathbf{E}^E(\boldsymbol{\rho}^E; z^E)$) in addition to the equivalent E_x distributions obtained from reference ray-tracing simulations. Subplots (b) and (e) depict results for which diffraction effects induced by the plano-convex lens and the subsequent free space propagation, are disregarded. These field components were obtained by relying only on pointwise operations for all involved field transforms applied between $\mathbf{E}^C(\boldsymbol{\rho}^C; z^C)$ and $\mathbf{E}^E(\boldsymbol{\rho}^E; z^E)$. Subplots (a) and (d) show the same electric field components in where all diffraction effects are then included. Additionally, in (c) and (f) we present equivalent E_x distributions obtained from non-sequential ray-tracing evaluations of the same system presented in Fig. 1(a). These distributions were obtained from ideal point sources with Gaussian-like and uniform amplitude distributions defined with a half angle of incidence equal to 40 degrees.

In the next step, the impact of diffraction and the field structures shown in Fig. 4 were evaluated in relation to the system's fiber in-coupling efficiency. For this, the $\mathbf{E}^f(\boldsymbol{\rho}^f; z^f)$ field components are compared against a reference fiber-field mode. The results of such a comparison can be observed in Fig. 5 in where we present focal plane field intensity distributions product of each dipole FDTD near-field source. Additionally, point spread function distributions corresponding to the reference Gaussian-like and uniform amplitude point sources obtained via sequential ray-tracing evaluations are displayed. For the subplots that correspond to our proposed approach, the shown fiber in-coupling efficiency values were obtained by directly using the focal plane complex amplitude distributions in combination with Eq. (4). As for the results corresponding to the ray-tracing evaluations, the displayed fiber in-coupling efficiency values were obtained from the ray distributions converging towards the systems focal planes.

From the results presented in Figs. 4 and 5 a few observations can be drawn. To start, there is a clear distinction in the obtained spatial symmetry shown in the electric field distributions from Fig. 4(a), (b), (d) and (e) with respect to the rotationally symmetric distributions corresponding to the idealized point source models used in the ray-tracing simulations. As already stated in Sec 4.1.1, for a dipole emitter positioned in close vicinity to dielectric interfaces, the obtained far-field distributions are strongly influenced by the relative dipole's position with respect to the interfaces and on the layered structure characteristics [25]. Such a specific nature of dipole

Optics EXPRESS

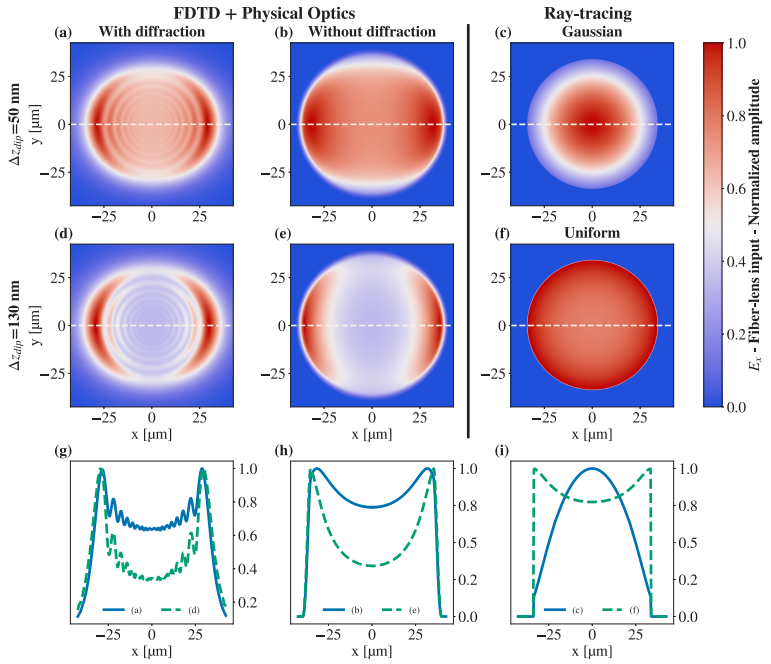

Fig. 4. E_x components at the fiber-lens entrance by neglecting (b), (e) and including (a), (d) diffraction effects obtained via the proposed FDTD + physical optics approach. Similarly, (c) and (f) display E_x equivalent field distributions obtained via non-sequential ray-tracing evaluations in combination with standard uniform and Gaussian-like amplitude point sources. Subplots (g), (h) and (i) present cross sections views of the electric field distributions across the white dashed lines shown in the 2D subplots.

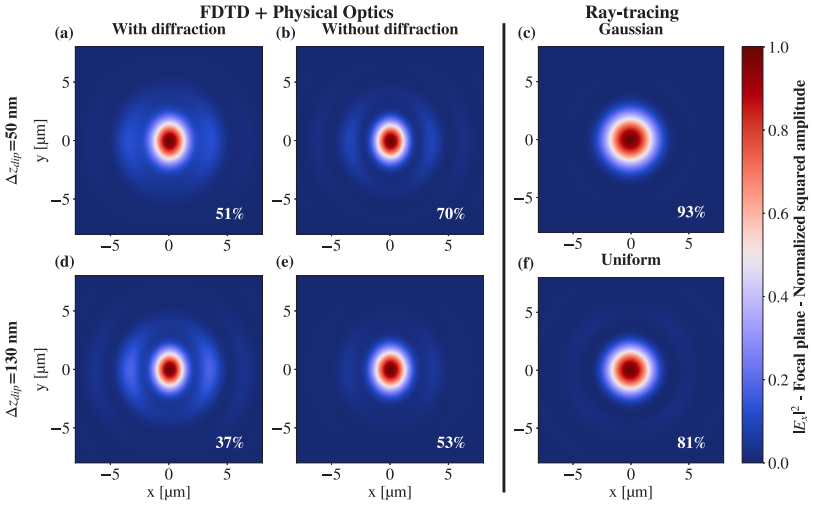

Fig. 5. Fiber-lens focal plane E_x intensity distributions associated to the field components shown in Fig. 4. Additionally, each subplot includes the computed fiber in-coupling efficiency value obtained via Eq. (4).

Optics EXPRESS

emitters in close proximity to finite interfaces cannot be captured by the assumed infinitesimal ideal point source models conventionally found within standard ray-tracing software packages. This demonstrates the importance of relying on additional numerical evaluations in order to extract far-field characteristics from point sources and directly consider these during the design of micro-optical components used as interfaces between point emitters and optical guiding elements such as waveguides or SMFs. As a second remark, it can be observed that the obtained fiber in-coupling efficiency for the Gaussian-like amplitude point source is higher in comparison to the value estimated for the uniform amplitude source model. This can be explained from the fact that an uniform pupil illumination results in a non Gaussian-like intensity distribution at the system's focal plane. In essence, for an uniform illumination profile, the strong interaction with the edges of a finite surface produce airy-like focal field patterns carrying higher energy density at secondary lobes in contrast to an ideal Gaussian function [33]. Similarly, by comparing the cross section views presented in Fig. 4(g) and (h) to the ones presented in Fig. 4(i) it is possible to comment on the causes behind the degraded coupling performance estimated for the same optical system in combination with the FDTD-based dipole source models. For these, the nonuniform and non Gaussian-like dipole far-field profiles result in stronger focal plane Ex differences with respect to the reference fiber Gaussian distribution. This difference, effectively reduces the required spatial overlap between the incident focal field profiles and the reference Gaussian fiber mode needed to guarantee a maximized fiber in-coupling efficiency [34].

Finally, by examining the cross sections presented in Fig. 4(g) and (h) and the results shown in the first and second column of Fig. 5, it can be concluded that the finite extent of the collimated beam generated by the plano-convex lens induces significant diffraction along the propagation towards the fiber-lens. Ultimately, this results in further optical performance degradation due to the non-smooth diffractive field structure. In such a case, diffraction cannot be ignored and must also be taken into account during the design and optimization of such compound micro-optical elements. At this point, we must mention that the insights obtained through our proposed approach, which combines rigorous simulations with physical optics methods, represent a departure from the ray-optics based analyses under uniform illumination conditions considered in previous related work [4,11,27]. Additionally, our methodology which offers a different framework for the study and analysis of compound single photon systems, is not limited to these and can easily be adapted to different combinations of nano-photonic structures [31] with integrated 3D printed micro-optical elements, allowing the extraction of valuable information not accessible through the referred approaches based on idealized point source models and ray-tracing analysis.

4.2. Dipole source within complex semiconductor structures

By fabricating nano-photonic structures around point-like emitters, it is possible to improve their emission characteristics. In this manner, high extraction efficiencies under narrow emission angles have been demonstrated, specially for Gaussian-like far-field distributions [8]. These type of emitters can also be combined with 3D printed micro-optics for the purpose of single photon coupling into SMFs. This ideas was previously introduced in [7], where the focus was on the use of a single lens attached to the facet of SMFs. In [7], the emitters field characteristics were approximated by point sources with Gaussian-like far-field distributions for the purpose of designing aspheric 3D printed SMF attached-lenses via sequential ray-tracing methods. In this section, we consider the inclusion of an additional micro-optical lens in direct contact to two semiconductor based optical nano-structures which were presented in [7] and that differ from a simple planar structure. To start, it is important to investigate possible near and far-field structural changes caused by the change in refractive index for the medium surrounding each nano-structure. Figure 6(a) and (d) show the geometry and material distributions for a circular Bragg grating (CBG) and a Mesa-based structure which are being considered in this case. The associated

Optics EXPRESS

design parameters can be obtained in Supplement 1. In [7], these structures were analyzed by only considering air as the medium on top of each structure at a wavelength of 930 nm. To the right of (a) and (d), near-field amplitude distributions extracted from each structure are displayed. These correspond to the original design case with air surrounding each nano structure and to the case in where the structures are surrounded by the same photopolymer considered in Sec. 4.1.1 (n=1.5025). Each near-field profile was obtained at a distance of 150 nm from the top semiconductor interface.

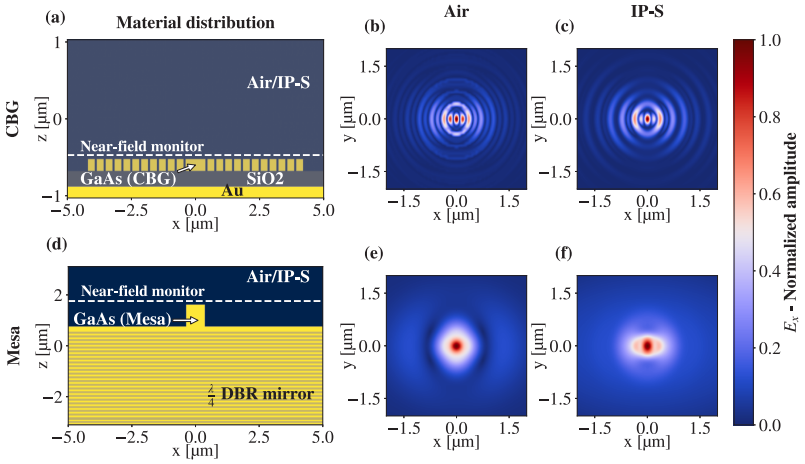

Fig. 6. (a) and (d) show the modeled CBG and Mesa material distributions. Next to these, near-field E_x components are displayed which were obtained via a FDTD near-field monitor positioned at a distance of 150 nm from the top semiconductor.

We then proceeded to the far-field propagation of the obtained near-field components via generalized far-field integral evaluations accordingly to what was presented in Sec. 3.2 and [26]. In Fig. 7(a),(b),(c) and (d) we present the far-field E_x distributions obtained from these evaluations. Additionally, in Fig. 7(e) we provide information on the far-field x-diameters for each field component. This was obtained by evaluating the extension for which the intensity dropped to a value smaller than 1% of the maximum. In a similar manner, from the IP-S based far-field information, we estimated the half-angles for which the far-field intensities dropped to a value of $1/e^2$ from their maximum in agreement with the definition used for a Gaussian-like far-field intensity profile. The values obtained for the CBG case were 11.74 and 7.77 degrees whereas for the Mesa structure case, half-angles equal to 42.53 and 33.41 degrees were estimated. As in Sec. 4.1, double lens micro-optical systems were optimized via sequential ray-tracing tools by approximating each IP-S based far-field distribution with an ideal rotationally symmetric Gaussian-like amplitude point source in agreement with the approach utilized in [7]. The used half-angles of emission were set to the largest $1/e^2$ half-angle from the values provided above. Details on the designed micro-optical systems can be found in Supplement 1. Following, we compare the fiber in-coupling efficiency values derived from reference ray-tracing based analysis to the results obtained via our proposed approach in accordance to the methodology presented in Sec. 3.2.

The obtained focal plane E_x intensity distributions and the corresponding fiber in-coupling efficiency values are shown in Fig. 8. From subplots (a) and (c) it is clear that for the CBG, its far-field distribution can be well approximated by a Gaussian-like field profile once the structure has been surrounded by the considered photopolymer. In this case, the generated far-field profile preserves its desired Gaussian-like amplitude characteristic resulting in high fiber in-coupling

Optics EXPRESS

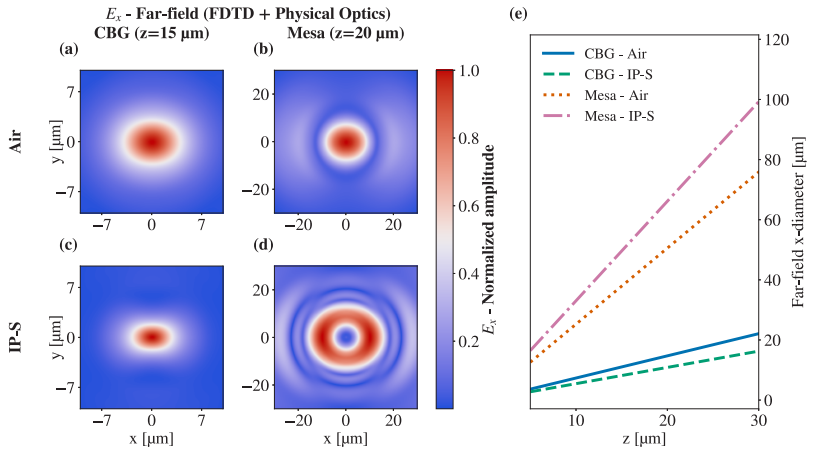

Fig. 7. Far-field E_x components obtained via generalized far-field integrals which correspond to the near-field E_x distributions shown in Fig. 6. Additionally, (e) shows the associated far-field E_x x-diameters evaluated as a function of the distance from the reference near-field monitors shown in Fig. 6

efficiency values. Additionally, even though a rotationally symmetric Gaussian distribution was used to approximate an astimatic beam profile, the obtained fiber in-coupling efficiency value is not severely impacted by this approximation. Finally, the narrow angular emission nature of such CBG structure, results in less significant influence of diffraction on the obtained fiber in-coupling efficiency, in contrast to the situation demonstrated in Sec. 4.1.2 for point emitters, which radiate more into larger angular extents.

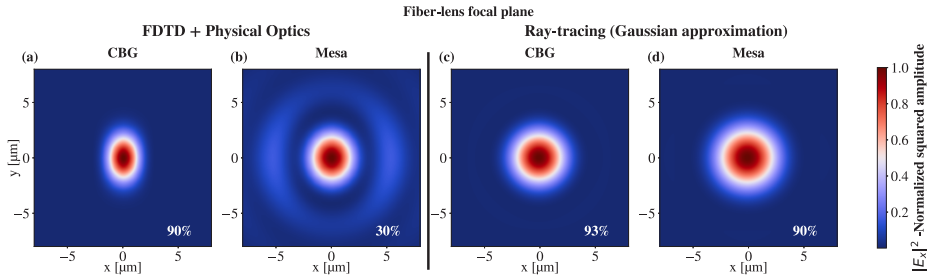

Fig. 8. Fiber-lens focal-plane $|E_x|^2$ components obtained after propagating (a), (b) IP-S based FDTD near field distributions shown in Fig. 6 and (c), (d) equivalent Gaussian fit approximate source distributions, through double lens micro-optical systems optimized via sequential ray-tracing tools.

As for the Mesa case, a larger discrepancy between the results presented in Fig. 8(b) and (d) can be observed. This can clearly be explained by noticing how for the Mesa, its far-field profile does not follow a Gaussian-like amplitude distribution once the nano-structure is surrounded by IP-S as shown in Fig. 7(d). As a result, such non Gaussian-like far-field characteristic highly impacts the fiber in-coupling efficiency in agreement to the discussion presented at the end of Sec. 4.1, rendering the utilized Gaussian source approximation model inaccurate in this case.

To conclude, we investigate the effects of introducing position offsets to the fiber-lens used in a double lens system and for a single fiber-lens configuration as the ones presented in [7]. These results are shown in Fig. 9, for which Eq. (4) is evaluated under different offset conditions. In

Optics EXPRESS

Fig. 9(a), the fiber in-coupling efficiency is evaluated by introducing a fiber-lens offset along z with respect to the nominal design values. Similarly, Fig. 9(b) and (c) present 2D maps for the fiber in-coupling efficiency values obtained by introducing xy-plane restricted offsets to the CBG's fiber-lenses at the nominal z position. From these evaluations, it is clear that a double lens system is less susceptible to position variations, whereas in the single lens case, the overlap decays to less than 50% of the maximum for z offsets larger than 3 μm and for values greater than 1 μm within the xy-plane. In general, a double-lens configuration can potentially enable excellent fiber coupling performance. Nevertheless, for this to be the case, it is also required to count with far-field source distributions that highly resemble Gaussian-like profiles. For emitter systems such as the CBG, this is directly provided by the nano-structure interaction with the point-emitter. Nevertheless, for other emitter architectures such as the Mesa-based system or the flat material configuration presented in Sec. 4.1, limited fiber in-coupling performance is to be expected as a consequence of the non Gaussian-like far-field source characteristics.

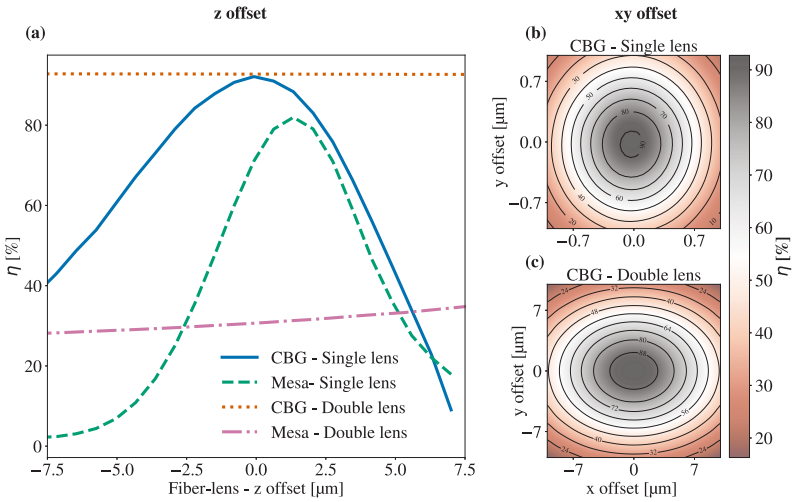

Fig. 9. Fiber-lens position offset influence on fiber in-coupling efficiency. (a) presents the evaluation for offsets along z with respect to the nominal lens z position and (b) and (c) displays coupling efficiency maps for offsets along x and y at the nominal fiber-lens z position. These evaluations were all performed via our proposed approach (FDTD + Physical Optics).

5. Conclusions

In this work, we propose a combined framework for modeling and analyzing micro-optical systems in the context of single photon sources. By integrating rigorous simulation approaches with fast physical optics methods, we provide a numerical scheme for studying such compound micro-optical systems that goes beyond the use of ray-tracing routines in combination with conventional point source models. It is well known that while focusing light into a SMF, high coupling efficiencies can only be obtained for Gaussian-like source amplitude distributions. Via the proposed method, we have observed that the non-ideal far-field characteristics possessed by different point-like emitters can strongly degrade the coupling performance of micro-optical systems designed in combination with standard point source models which are typically found within common ray-tracing software packages. The use of such conventional models can result in optical performance overestimation, which at the end, cannot be matched under experimental conditions. This demonstrates the importance of relying on rigorous simulation methods in order to validate the use of such common source approximation models for describing different

Optics EXPRESS

SPSs far-field distributions. Also, we have demonstrated that the use of fast physical optic methods allows the propagation of extracted near-field components through multiple micro-optical interfaces, providing an efficient manner to identify the relevance of different physical aspects such as diffraction, which can further contribute to a micro-optical system's overall fiber in-coupling performance degradation. Finally, our proposed numerical approach benefits from an inherent modeling modularity, making it sufficiently flexible to model multiple nano-photonic systems in combination with a wide range of micro-optical interfaces. Furthermore, it can potentially be extended from the scope of modeling and analyzing such compound systems, to the design and optimization of micro-optical components tailored to the specific far-field characteristics of various point source emitters, facilitating in this manner compact high performance integrated single photon sources.

Funding. Deutsche Forschungsgemeinschaft (431314977/GRK2642).

Acknowledgments. We gratefully acknowledge LightTrans GmbH for providing access to the VirtualLab Fusion software package. Funded by the Deutsche Forschungsgemeinschaft (DFG, German Research Foundation) - 431314977/GRK2642.

Disclosures. The authors declare no conflicts of interest.

Data Availability. Data underlying the results presented in this paper are not publicly available at this time but may be obtained from the authors upon reasonable request.

Supplemental document. See Supplement 1 for supporting content.

References

1. Y. Arakawa and M. J. Holmes, "Progress in quantum-dot single photon sources for quantum information technologies: A broad spectrum overview," Appl. Phys. Rev. **7**(2), 021309 (2020).
2. H. Kumano, T. Harada, I. Suemune, H. Nakajima, T. Kuroda, T. Mano, K. Sakoda, S. Odashima, and H. Sasakura, "Stable and efficient collection of single photons emitted from a semiconductor quantum dot into a single-mode optical fiber," Appl. Phys. Express **9**(3), 032801 (2016).
3. K. Żołnacz, A. Musiał, N. Srocka, *et al.*, "Method for direct coupling of a semiconductor quantum dot to an optical fiber for single-photon source applications," Opt. Express **27**(19), 26772–26785 (2019).
4. L. Bremer, K. Weber, S. Fischbach, S. Thiele, M. Schmidt, A. Kaganskiy, S. Rodt, A. Herkommer, M. Sartison, S. L. Portalupi, P. Michler, H. Giessen, and S. Reitzenstein, "Quantum dot single-photon emission coupled into single-mode fibers with 3d printed micro-objectives," APL Photonics **5**(10), 106101 (2020).
5. P.-I. Dietrich, M. Blaicher, I. Reuter, M. Billah, T. Hoose, A. Hofmann, C. Caer, R. Dangel, B. Offrein, U. Troppenz, M. Moehrle, W. Freude, and C. Koos, "In situ 3d nanoprinting of free-form coupling elements for hybrid photonic integration," Nat. Photonics **12**(4), 241–247 (2018).
6. T. Gissibl, S. Thiele, A. Herkommer, and H. Giessen, "Sub-micrometre accurate free-form optics by three-dimensional printing on single-mode fibres," Nat. Commun. **7**(1), 11763 (2016).
7. L. Bremer, C. Jimenez, S. Thiele, K. Weber, T. Huber, S. Rodt, A. Herkommer, S. Burger, S. Höfling, H. Giessen, and S. Reitzenstein, "Numerical optimization of single-mode fiber-coupled single-photon sources based on semiconductor quantum dots," Opt. Express **30**(10), 15913 (2022).
8. H. Abudayyeh, B. Lubotzky, A. Blake, J. Wang, S. Majumder, Z. Hu, Y. Kim, H. Htoon, R. Bose, A. V. Malko, J. A. Hollingsworth, and R. Rapaport, "Single photon sources with near unity collection efficiencies by deterministic placement of quantum dots in nanoantennas," APL Photonics **6**(3), 036109 (2021).
9. S. Kolatschek, C. Nawrath, S. Bauer, J. Huang, J. Fischer, R. Sittig, M. Jetter, S. L. Portalupi, and P. Michler, "Bright purcell enhanced single-photon source in the telecom o-band based on a quantum dot in a circular bragg grating," Nano Lett. **21**(18), 7740–7745 (2021).
10. C.-M. Lee, M. A. Buyukkaya, S. Aghaeimeibodi, A. Karasahin, C. J. K. Richardson, and E. Waks, "A fiber-integrated nanobeam single photon source emitting at telecom wavelengths," Appl. Phys. Lett. **114**(17), 171101 (2019).
11. M. Sartison, K. Weber, S. Thiele, L. Bremer, S. Fischbach, T. Herzog, S. Kolatschek, M. Jetter, S. Reitzenstein, A. Herkommer, P. Michler, S. L. Portalupi, and H. Giessen, "3d printed micro-optics for quantum technology: Optimised coupling of single quantum dot emission into a single-mode fibre," Light: Adv. Manuf. **2**(2), 103 (2021).
12. A. Asadollahbaik, S. Thiele, K. Weber, A. Kumar, J. Drozella, F. Sterl, A. M. Herkommer, H. Giessen, and J. Fick, "Highly efficient dual-fiber optical trapping with 3d printed diffractive fresnel lenses," ACS Photonics **7**(1), 88–97 (2020).
13. S. Ristok, P. Flad, and H. Giessen, "Atomic layer deposition of conformal anti-reflective coatings on complex 3d printed micro-optical systems," Opt. Mater. Express **12**(5), 2063 (2022).
14. J. Große, M. von Helversen, A. Koulas-Simos, M. Hermann, and S. Reitzenstein, "Development of site-controlled quantum dot arrays acting as scalable sources of indistinguishable photons," APL Photonics **5**(9), 096107 (2020).

Optics EXPRESS

15. T. Gissibl, S. Thiele, A. Herkommer, and H. Giessen, "Two-photon direct laser writing of ultracompact multi-lens objectives," Nat. Photonics **10**(8), 554–560 (2016).
16. A. Toulouse, J. Drozella, S. Thiele, H. Giessen, and A. Herkommer, "3d-printed miniature spectrometer for the visible range with a 100 μ m × 100 μ m footprint," Light: Adv. Manuf. **2**(1), 20 (2021).
17. W. Zhang, H. Zhang, C. J. R. Sheppard, and G. Jin, "Analysis of numerical diffraction calculation methods: from the perspective of phase space optics and the sampling theorem," J. Opt. Soc. Am. A **37**(11), 1748–1766 (2020).
18. A. Wyrowski, F. Drauschke, A. Aagedal, and H. Pfeil, "Analysis of optical elements with the local plane-interface approximation," Appl. Opt. **39**(19), 3304–3313 (2000).
19. R. Shi, C. Hellmann, and F. Wyrowski, "Physical-optics propagation through curved surfaces," J. Opt. Soc. Am. A **36**(7), 1252–1260 (2019).
20. P.-I. Schneider, N. Srocka, S. Rodt, L. Zschiedrich, S. Reitzenstein, and S. Burger, "Numerical optimization of the extraction efficiency of a quantum-dot based single-photon emitter into a single-mode fiber," Opt. Express **26**(7), 8479–8492 (2018).
21. P. Chanhyung, S. Jeongmin, K. Sanmun, L. Songju, P. Juho, P. Jaehyeok, P. Sehong, Y. Seunghyup, and J. MinSeok, "Fast and rigorous optical simulation of periodically corrucated light-emitting diodes based on a diffraction matrix method," Opt. Express **31**(12), 20410–20423 (2023).
22. C. Michiel K., M. Herman, P. Lieven, P. Patrick, D. G. Harry, M. Jan M., and N. Kristiaan, "RCWA and FDTD modeling of light emission from internally structured OLEDs," Opt. Express **22**(S3), A589–A600 (2014).
23. A. F. Oskooi, D. Roundy, M. Ibanescu, P. Bermel, J. D. Joannopoulos, and S. G. Johnson, "Meep: A flexible free-software package for electromagnetic simulations by the fdtd method," Comput. Phys. Commun. **181**(3), 687–702 (2010).
24. P. Munro and P. R. T. Torok, "Rigorous near to far field transformations for vectorial diffraction calculations and its numerical implementation," J. Opt. Soc. Am. A **23**(3), 713–722 (2006).
25. L. Novotny, "Allowed and forbidden light in near-field optics i a single dipolar light source," J. Opt. Soc. Am. A **14**(1), 91 (1997).
26. Z. Wang, O. Baladron-Zorita, C. Hellmann, and F. Wyrowski, "Generalized far-field integral," Opt. Express **29**(2), 1774–1787 (2021).
27. S. Fischbach, A. Schlehahn, A. Thoma, N. Srocka, T. Gissibl, S. Ristok, S. Thiele, A. Kaganskiy, A. Strittmatter, T. Heindel, S. Rodt, A. Herkommer, H. Giessen, and S. Reitzenstein, "Single quantum dot with microlens and 3d-printed micro-objective as integrated bright single-photon source," ACS Photonics **4**(6), 1327–1332 (2017).
28. K. Serrels, "Solid immersion lens applications for nanophotonic devices," J. Nanophotonics **2**(1), 021854 (2008).
29. Z. Wang, O. Baladron-Zorita, C. Hellmann, and F. Wyrowski, "Theory and algorithm of the homeomorphic fourier transform for optical simulations," Opt. Express **28**(7), 10552–10571 (2020).
30. R. Shi, Z. Wang, S.-T. Hung, C. Hellmann, and F. Wyrowski, "Numerical analysis of tiny-focal-spot generation by focusing linearly, circularly, and radially polarized beams through a micro/nanoparticle," Opt. Express **29**(2), 2332–2347 (2021).
31. R. Shi, N. Janunts, C. Hellmann, and F. Wyrowski, "Vectorial physical-optics modeling of fourier microscopy systems in nanooptics," J. Opt. Soc. Am. A **37**(7), 1193–1205 (2020).
32. Physical optics simulation and design software "Wyrowski VirtualLab Fusion".
33. V. Mahajan, "Uniform versus Gaussian beams: a comparison of the effects of diffraction, obsuration, and aberrations," J. Opt. Soc. Am. A **3**(4), 470–485 (1986).
34. M. H. Lee, J. Y. Jo, D. W. Kim, Y. Kim, and K. H. Kim, "Comparative study of uniform and nonuniform grating couplers for optimized fiber coupling to silicon waveguides," J. Opt. Soc. Korea **20**(2), 291–299 (2016).